JOURNAL OF CATALYSIS **160,** 171–182 (1996)
ARTICLE NO. 0136

Yttria-Stabilized Zirconia Supported Copper Oxide Catalyst

II. Effect of Oxygen Vacancy of Support on Catalytic Activity for CO Oxidation

Wei-Ping Dow and Ta-Jen Huang[1]

Department of Chemical Engineering, National Tsing Hua University, Hsinchu, Taiwan 300, Republic of China

Received March 20, 1995; revised October 20, 1995; accepted January 23, 1996

Copper oxide was supported on yttria-stabilized zirconia (YSZ) and γ-alumina, respectively, using impregnation methods. The supported copper oxide catalysts were characterized by temperature-programmed reduction. The catalytic activity of copper oxide supported on YSZ for CO oxidation was measured and compared with those supported on γ-alumina and with commercial γ-alumina supported precious metals (PMs) (i.e., Pd and Pt). Results of the activity tests indicated that CuO/YSZ catalysts can exhibit PM-like behaviors such as the light-off characteristic and the hysteresis phenomenon but CuO/γ-alumina catalysts cannot do so. The significant and conspicuous activity enhancement of the YSZ supported copper oxide has been ascribed to the modification of reaction mechanism due to the surface oxygen vacancy of YSZ. An active center composed of an interfacial Cu^+ ion and a surface oxygen vacancy of YSZ and formed by an interfacial metal oxide–support interaction is proposed to explain the activity enhancement. These interfacial active centers could provide a second reaction pathway for CO oxidation via the so-called "metal–support interfacial reaction" step, for which the turnover frequency is much higher than that of redox cycle mechanism operated on the CuO/γ-alumina catalyst. These interfacial active centers can be destroyed by chlorine addition due to blocking of the surface oxygen vacancies of YSZ by the strongly adsorbed chlorine. The reaction mechanism and catalytic behavior of PM/γ-alumina, CuO/γ-alumina, and CuO/YSZ catalysts are compared and discussed.

1. INTRODUCTION

After the concept of strong metal–support interaction (SMSI) is proposed, the role of support, especially reducible support, becomes increasingly important. It not only can act as a carrier but also may give some kind of contribution in catalytic reactions. For example, the selectivity and reaction rate of CO hydrogenation has been significantly enhanced by SMSI (1, 2). However, up to date, no conclusive explanation has been given for this phenomenon.

For CO oxidation, metal–support interaction also exhibits a marked effect on activity enhancement. The well-known catalysts are noble metals supported on cerium oxide for automobile emission control (3–5). On these catalysts, a new concept, interfacial metal–support interaction (IMSI), is proposed to interpret the reason for their high activity in CO oxidation when metals are supported on cerium oxide and oxygen-ion conducting support (5 –12). Their common theory and explanation are that the interfacial perimeter between metal particle and support can provide very active centers due to the generation of oxygen vacancies on the support. When the interfacial active centers are formed, they can change the reaction mechanism and kinetic order as well as reduce the activation energy for CO oxidation (11–14).

In fact, a similar concept of IMSI, which is caused by the surface oxygen vacancies of support, had been proposed by many authors (15, 16) to explain the high selectivity of CO hydrogenation over metal/TiO_2 catalysts. Recently, Sanchez and Gazquez (17) systematically elucidated the role of support oxygen vacancy on SMSI. They pointed out that a proposed model of oxygen vacancy occupancy by metal atoms can be equally applicable to different oxide systems, but the resulting effects may vary profoundly depending on the nature of support. However, they never consider whether the oxygen vacancies of the oxide support may take part in catalysis. Many investigations have shown that the oxygen vacancies of metal oxides such as vanadium oxide (18, 19), copper oxide (20, 21), and superconducting oxides (22, 23) play an important role in CO oxidation and N_2O decomposition. More recently, Ekerdt and co-workers (24–26) confirmed that the active site for CO hydrogenation over Y_2O_3-stabilized ZrO_2 (YSZ) and CaO-stabilized ZrO_2 (CSZ) is an oxygen vacancy. They further pointed out that at higher oxygen vacancy mobility, higher selectivity and reaction rate were realized.

Precious metals (PMs) such as platinum, palladium, and rhodium have been demonstrated to be the most efficient three-way catalysts (TWCs) used to control automotive exhaust (27, 28). However, attention has also been given to base metals due to the limited availability of PMs. Among the base metals, copper has been explored as a possible

[1] To whom correspondence should be addressed.

0021-9517/96 $18.00

palladium and platinum substitute for NO_x reduction and CO oxidation in TWCs (28–32). Nevertheless, some disadvantages of the base metals such as no light-off characteristic, spinel formation with support, considerable requirement of copper loading, poor poison resistance, and no chemisorption-type reaction mechanism have not yet been overcome completely (27).

Their turnover frequencies (TOF) are lower than those of PMs (27), and this leads to a poor light-off behavior and a considerable requirement of base-metal loading (27). The lower TOF can be associated with the mechanism. In general, CO oxidation over base-metal oxide catalysts belongs to the Mars–van Krevelen redox mechanism (18–20, 22, 28, 33–35). In order to improve the catalytic activity of copper catalyst for CO oxidation and NO reduction, many researchers have adopted different methods to modify the reactivity. These include high-temperature reduction treatment (29, 30), addition of chromium (20, 31, 36, 37), and addition of a little platinum (38). However, the reaction mechanism in which CO reacts with the lattice oxygen of copper oxide instead of chemisorbed oxygen cannot be changed still.

Hence, it is conceivable that if one can modify the reaction mechanism by means of a new active center, which does not go through the redox mechanism but through a rapid reaction path, perhaps the catalytic activity of copper catalysts can compete with those of PMs for CO oxidation. A feasible way is to choose a proper support that leads to some kind of interfacial metal oxide–support interaction (IMOSI) or synergistic effect. Methanol oxidation over supported vanadium oxide catalysts (39) is a typical instance.

In our previous work (40), we have made a comparative TPR study of CuO/γ-alumina and CuO/YSZ catalysts. It was found that two TPR peaks, β and γ, can be observed in the TPR patterns of CuO/γ-alumina catalyst, while four TPR peaks, α_1 and α_2, as well as β and γ, can be distinguished on the TPR curves of CuO/YSZ catalyst. The β peak has been attributed to the reduction of highly dispersed copper oxide species, which include isolated copper ions, weak magnetic associates, and small two- and three-dimensional clusters. The γ peak has been ascribed to the reduction of bulk-like CuO phases that include large clusters and bulk CuO. The α_1 and α_2 peaks, of which the temperatures are much lower than that of β and γ peak have been attributed to the hydrogen uptake of nested oxygen ions (NOIs) and temptable oxygen ions (TOIs) of the YSZ supported copper oxide (40), respectively. These oxygen ions are the interface-boundary terminal oxygen ions of supported copper oxide but have different environment and interaction with the surface oxygen vacancies of YSZ support. The former case, NOI, results from the function of oxygen-ionic transport of the YSZ support; the latter case, TOI, results from the oxygen vacancy of YSZ acting as the Lewis acid sites (40).

It is believed that these copper oxide species should have different reactivity due to their different environment and interaction with the support. Hence, in this work, we study the catalytic activity of CuO/YSZ catalyst for CO oxidation and try to find out which copper oxide species is the predominant contributor in activity enhancement.

This work reports the effect of IMOSI on catalytic activity of supported copper oxide catalyst. These investigations include the IMOSI effect on the light-off behavior of CO oxidation over copper oxide and the reaction mechanism. Two commercial PM catalysts, Pt/γ-alumina and Pd/γ-alumina, were employed for comparison of catalytic activity. Results indicate that the IMOSI can modify the reaction mechanism of CO oxidation on the YSZ supported copper oxide catalyst and thus significantly improve the light-off behavior of CO oxidation on the copper oxide catalyst even better than that of PM. The considerable copper loading requirement over traditional support (e.g., alumina) can also be overcome by the IMOSI effect after copper oxide is supported on the oxygen-ion conducting YSZ support.

2. EXPERIMENTAL

Catalyst preparation and characterization. The supported copper oxide catalysts with various copper loadings were prepared by the conventional impregnation method on YSZ and γ-alumina powder. Details of the preparation have been described elsewhere (40). The properties of the freshly calcined catalysts such as BET areas have also been reported in Part I (40) of this work. Two commercial PM catalysts employed for comparison of catalytic activity were purchased from Strem Chemicals (0.5 wt% Pt/γ-alumina and 0.5 wt Pd/γ-alumina, 90–95 m^2/g, 150–200 mesh).

In order to reveal the reason for activity enhancement and the structure of active species of the CuO/YSZ catalysts, HCl was added to impregnating aqueous solutions of copper nitrate to produce CuO/YSZ catalysts that contained chlorine. Three chlorine-containing CuO/YSZ catalysts were made with different mole percentages of chlorine with respect to copper content, i.e., Cl/(Cl + Cu), during impregnation. For the case of 0.6 wt% Cu/YSZ catalyst, two chlorine-containing samples were prepared with chlorine content of 10 and 70 mol%, respectively. For the case of 1.5 wt% Cu/YSZ catalyst, only one chlorine-containing sample was prepared with chlorine content of 10 mol%. The chlorine contents were those during impregnation. After the chlorine-containing catalysts were calcined in air at 500°C, some chlorine might be removed from the catalysts due to formation of Cl_2 and HCl. Accordingly, the Cl/Cu ratios of the chlorine-containing catalysts became unknown after calcination.

Apparatus and method of activity test. The activities of the catalysts were measured in a continuous flow reactor at

atmospheric pressure. The reactor was an 8-mm-i.d. quartz U-tube. Two type-K thermocouples were employed. One was placed at the outside wall of the reactor tube to control the temperature of the furnace; the other was inserted into the catalyst powder to monitor the temperature of the catalyst bed.

Activity-tested samples charged in the catalyst bed were classified into two categories. One was constant sample weight; the other was constant metal weight. For the case of constant sample weight, every tested sample packed in the catalyst bed had a same weight of 0.1 g. Accordingly, the absolute amount of copper in the catalyst bed varied. For the case of constant metal weight, every tested sample packed in the catalyst bed possessed different weight in order to maintain a same copper weight for each run. The copper weight charged in the catalyst bed was fixed at 1 mg for the γ-alumina support, while the copper weight was fixed at 0.4 mg for the case of YSZ support. The main purpose of the classification was to control the absolute amount of the different supported copper oxide species in the catalyst bed.

All the activity-tested samples were diluted with α-alumina powder (Aldrich, 150–325 mesh) in order to reduce the heat effect generated by CO oxidation. In addition, the volume of the test sample could held constant by means of the powder dilution. Therefore, the space velocity, volume flow rate of gas/volume of catalyst powder, could be maintained to be the same for all test samples.

The comparison of catalytic activity was carried out by measuring the percentage conversion of CO oxidation as a function of temperature ("light-off" test). These curves of conversion versus temperature can serve as a convenient activity indicator for the practical application of these catalysts. Before each activity test, the catalyst in the reactor was dried in air at 150°C for 1.5 h in order to remove the moisture adsorbed on the catalyst. The light-off test was performed under an oxygen-rich condition with a gas mixture composed of 3% O_2 plus 2% CO in argon and with a total flow rate of 300 ml/min. The flows of the reactant gases, CO (CP Grade, Air Products), O_2 (99.995%), and Ar (99.9995%), were adjusted by mass flow controllers (Hastings, Model HFC-202). The CO gas used had been purified by passing through a column packed with molecular sieve 5A and then through a filter to remove impurities (e.g., metal carbonyl) and moisture. The reactor outflow was analyzed on line by a gas chromatograph (Shimadzu, Model GC-8A) with a thermal conductivity detector, a CO analyzer (Beckman, Model 880), and an oxygen analyzer (Beckman, Model 755A). Both the signals of the CO analyzer and the temperatures of the catalyst bed were transmitted to a Y-t recorder (Yokogowa, Model LR-4110).

During the light-off test, the temperature of furnace was raised from 120°C to a desired one in steps of 10–15°C and controlled by a temperature controller (Eurotherm, Model 812). Between two 10–15 °C steps the temperature of furnace was held constant until the temperature of the catalyst bed had reached a steady state. At that moment, the CO and O_2 concentration of the reactor outlet were simultaneously sampled with the gas chromatograph and thus the CO conversion could be accordingly obtained. Usually, it would take 30–60 min to reach each steady state. For several light-off tests, the results of decreasing temperature were also recorded in order to investigate the hysteresis phenomenon of activity versus temperature.

Temperature-programmed reduction (TPR). In our previous work (40), we reported detailed TPR studies of CuO/YSZ catalysts and proposed mechanisms for the reduction of YSZ supported copper oxide. For the sake of investigating how the YSZ support can enhance the catalytic activity of a copper oxide catalyst for CO oxidation, TPR tests of several chlorine-free and chlorine-doped CuO/YSZ catalysts were carried out. Moreover, the reduction mechanisms proposed in our previous work can also be further confirmed by the addition of chlorine. The apparatus and method of TPR has been described in Part I (40) of this work.

3. RESULTS

3.1. Steady-State Activity Test

The steady-state activities of CuO/γ-alumina catalysts are shown in Fig. 1. It is seen that the catalyst activity varies with the copper loading and has a maximum value at 7.5 wt% Cu. A similar result was also obtained by Severino *et al.* (36).

Figure 1 also shows the relationship between the activity and the percentage of TPR peak area. The relative fractions

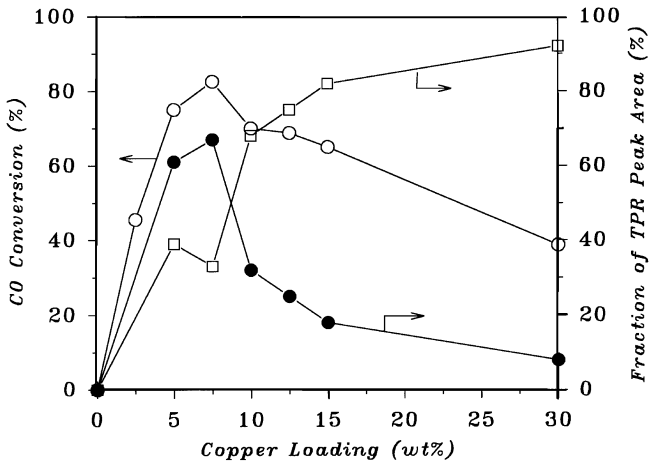

FIG. 1. The relationships among the steady-state activity, TPR peak area, and copper loading of CuO/γ-alumina catalyst. Activity-tested conditions: constant copper weight of 1 mg; 3% O_2 + 2% CO in Ar; total flow rate, 300 ml/min; temperature, 280°C; space velocity, 120,000 h^{-1}. (○) CO conversion, (●) fraction of β-peak area, (□) fraction of γ-peak area.

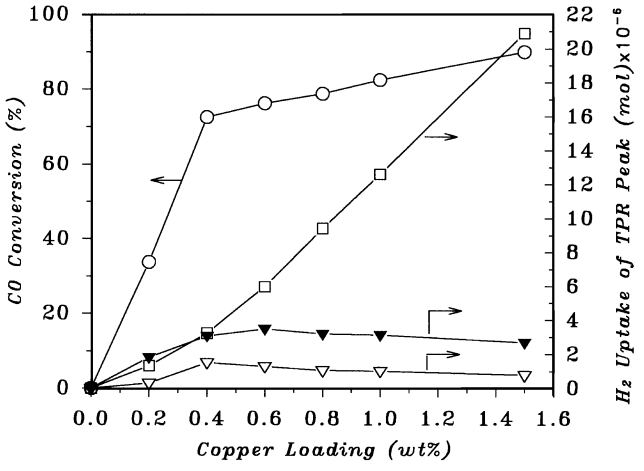

FIG. 2. The relationships among the steady-state activity, hydrogen uptake of TPR peak area, and copper loading of CuO/YSZ catalyst. Activity-tested conditions: constant sample weight of 100 mg; temperature, 220°C; space velocity, 72,000 h^{-1}; the rest is the same as that of Fig. 1. (○) CO conversion, (▽) hydrogen uptake of α_1-peak area, (▼) hydrogen uptake of α-peak area, (□) hydrogen uptake of $\beta+\gamma$-peak area.

of the TPR peak area were obtained from our previous results (40). Obviously, the trend of catalytic activity varying with the copper loading is analogous to that of β-peak area fraction. On the other hand, the variation of catalyst activity with the copper loading shown in Fig. 1 is independent of that of γ-peak area fraction. This implies that the β-peak copper oxide species are predominant contributors in catalytic activity of the CuO/γ-alumina catalysts. It has been shown that the β-peak copper oxide species are reduced more easily that γ-peak species (40); hence, the catalytic activity of CuO/γ-alumina catalyst should be associated with the reducibility of alumina supported copper oxide.

Figure 2 shows the relationships among steady state activity, hydrogen uptake for different TPR peaks, and different copper loading for CuO/YSZ catalyst under a tested condition of constant sample weight. The hydrogen consumptions of different TPR peak areas were also obtained from our previous work (40). Considering the variation of catalytic activity with increasing copper loading, there is a turning point at 0.4 wt% Cu. Below this copper loading, the catalytic activity has a drastic change with copper loading, while beyond 0.4 wt% Cu the catalytic activity varies mildly with increasing copper loading.

To combine the results of hydrogen uptake of different TPR peak areas, one can find out that the turning point of activity exactly occurs at the maximum value of α_1-peak area, of which the copper loading is 0.4 wt% (40). On the other hand, the maximum values of α- and $\beta+\gamma$-peak areas appear at 0.6 and 1.5 wt%, respectively (40). It should be noted that the hydrogen uptake of $\beta+\gamma$-peak area increases markedly when the copper loading is higher than 0.4 wt%. Therefore, it is believed that the predominant contributors in the activity of CuO/YSZ catalyst should be the α_1-peak copper oxide species, but the contribution of $\beta+\gamma$-peak copper oxide species in activity is not completely negligible when their amounts are large enough.

In order to confirm that the α_1-peak copper oxide species are the predominant active species of CuO/YSZ catalyst for CO oxidation, an activity-tested condition of constant copper weight is carried out. These results are shown in Fig. 3. Indeed, the variation trend of activity and α_1-peak area is synchronous with increasing the copper loading. Both the activity and the hydrogen uptake of α_1-peak area have a maximum value at 0.4 wt% Cu. Furthermore, the catalytic activity is independent of either the fraction of α-peak copper oxide species or that of $\beta+\gamma$-peak ones. These suggest that the catalytic activity of CuO/YSZ catalyst is dominated by the α_1-peak copper oxide species and depends on its amount. This is to say that the catalytic reaction is associated with the surface oxygen vacancy of YSZ support, because the generation of α_1-peak is relevant to the surface oxygen vacancy of YSZ support (40).

3.2 Light-Off Test

Hightower (27) has reported that PM catalysts such as platinum and palladium have a so-called "light-off" characteristic for CO oxidation, whereas base metal catalysts such as γ-alumina supported copper oxide catalyst do not. This typical behavior has also been obtained in this work as shown in Fig. 4. For the PM catalysts, one cannot obtain a CO conversion between 10 and 90%, while one can obtain a medium CO conversion over the CuO/γ-alumina catalyst. It should be emphasized that the 7.5 wt% Cu/γ-alumina catalyst chosen for this test has been shown in Fig. 1 to be

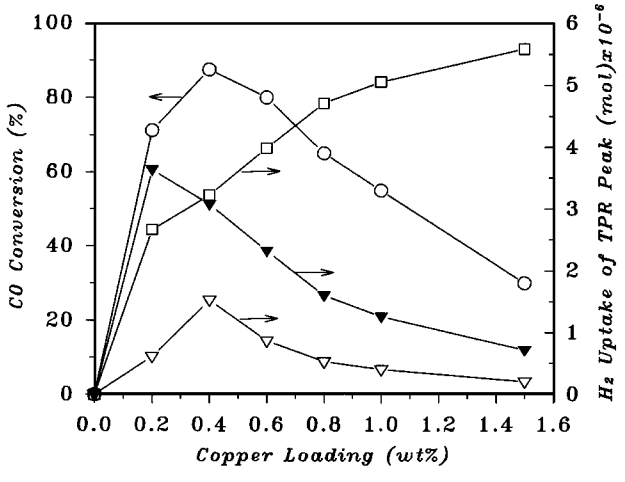

FIG. 3. The relationships among the steady-state activity, hydrogen uptake of TPR peak area, and copper loading of CuO/YSZ catalyst. Activity-tested conditions: constant copper weight of 0.4 mg; space velocity, 90,000 h^{-1}. The rest is the same as that of Fig. 2. Symbols are as in Fig. 2.

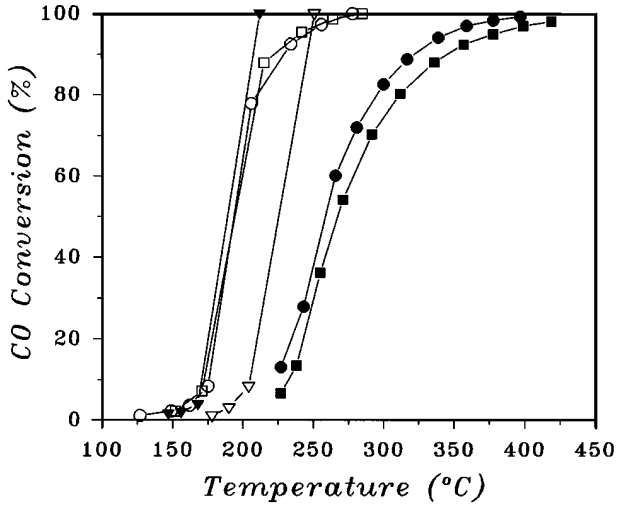

FIG. 4. Light-off plots of various catalysts. Operation conditions: 3% O_2 + 2% CO in Ar; total flow rate, 300 ml/min; space velocity, 90,000 h^{-1}. Catalysts: (▼) 0.5 wt% Pd/γ-alumina; Pd weight, 0.4 mg; (▽) 0.5 wt% Pt/γ-alumina; Pt weight, 0.4 mg; (■) 5 wt% Cu/γ-alumina; Cu weight, 1 mg; (●) 7.5 wt% Cu/γ-alumina; Cu weight, 1 mg; (○) 0.4 wt% Cu/YSZ; Cu weight, 0.4 mg; (□) 1.5 wt% Cu/YSZ; Cu weight, 1.5 mg.

the best one for CO oxidation among the CuO/γ-alumina catalysts of different copper loading. The difference in the catalytic behavior between the PM catalyst and the CuO/γ-alumina catalyst has been attributed to the difference in reactivity of the active sites and reaction mechanisms (27, 28).

An interesting and surprising result is obtained over CuO/YSZ catalyst, also shown in Fig. 4. The CuO/YSZ catalyst also exhibits a light-off characteristic and behaves like the PM catalyst. Considering the CO conversions at a given temperature shown in Fig. 4, the BET areas of the supports (i.e., 10.1 m^2/g for CuO/YSZ, 169.5 m^2/g for CuO/γ-alumina, and 90–95 m^2/g for PM/γ-alumina), and the corresponding dispersions of the supported PMs or copper oxides, the catalytic activity of CuO/YSZ catalyst is much better than that of the CuO/γ-alumina catalyst and even better than that of the PM catalyst tested. We believe that a new reaction mechanism, which is different from that of CuO/γ-alumina catalyst, is operating on the CuO/YSZ catalyst, because there is a marked discrepancy in the catalytic behavior of these base metal catalysts.

It is worthy to note that the jump-off temperatures of the light-off curves of the CuO/YSZ catalysts shown in Fig. 4 are near 175°C, which are very close to the reduction temperatures of α_1-peak copper oxide species (40). In addition, the jump-off temperatures of the light-off curves of the CuO/YSZ catalysts are approximately independent of copper loading. The typical results can be seen in Fig. 4. This suggests that the light-off characteristic of CuO/YSZ catalyst in CO oxidation is associated with the reduction of α_1-peak copper oxide species.

3.3 Hysteresis Phenomenon

In order to realize the difference in reaction mechanism and adsorption character between the γ-alumina supported PMs and copper oxide, the fall-off curves of decreasing reaction temperature in the light-off test are recorded and shown in Fig. 5. In practice, these are typical results and behaviors of CO oxidation over the γ-alumina supported PM and copper oxide catalysts.

It is obvious that the hysteresis loop occurs only on the PM catalysts. For CuO/γ-alumina catalyst, the rising curve should overlap the fall-off curve, which exhibits a "reversible" process, as long as the highly dispersed copper oxide species do not sinter during increasing the reaction temperature. Hence, a slight loss of conversion of the 7.5 wt% Cu/γ-alumina during decreasing reaction temperature is due to the sintering of dispersing copper oxide species.

From the results of Fig. 5, it can be observed that after the reaction temperature has been decreased from the point of 100% CO conversion for ca. 50°C, the CO conversion can still be maintained at 100%. On the other hand, γ-alumina supported copper oxide catalyst cannot do so, its CO conversion reduces with decreasing reaction temperature. Many studies have reported that the mechanism for CO oxidation over the PM catalysts is a Langmuir–Hinshelwood type mechanism (41–43), while the Mars–van Krevelen mechanism is operative on the copper oxide catalyst (20, 28, 34, 35). Hence, it is believed that the hysteresis phenomena of CO oxidation in the light-off test is not only related to the chemisorption-type reaction mechanism but are also associated with very high TOFs of the active sites.

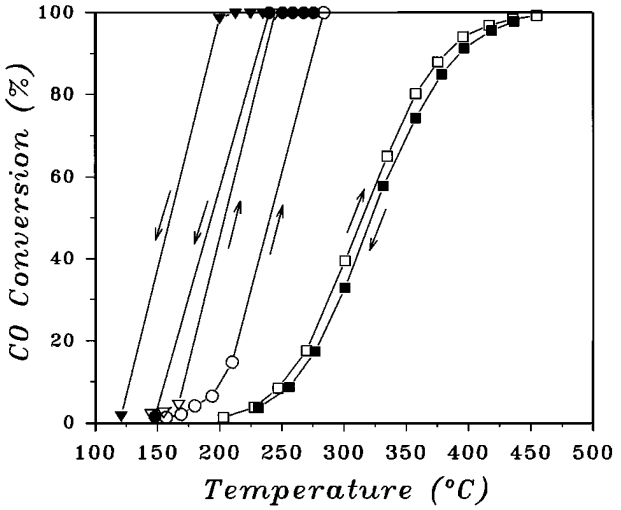

FIG. 5. Hysteresis phenomenon in the light-off test. Operation conditions: constant metal weight of 0.6 mg; space velocity, 60,000 h^{-1}; the rest is the same as that of Fig. 4. Catalysts: (▽, ▼) 0.5 wt% Pd/γ-alumina, (○, ●) 0.5 wt% Pt/γ-alumina, (□, ■) 7.5 wt% Cu/γ-alumina. Open symbols, increasing temperature; filled symbols, decreasing temperature.

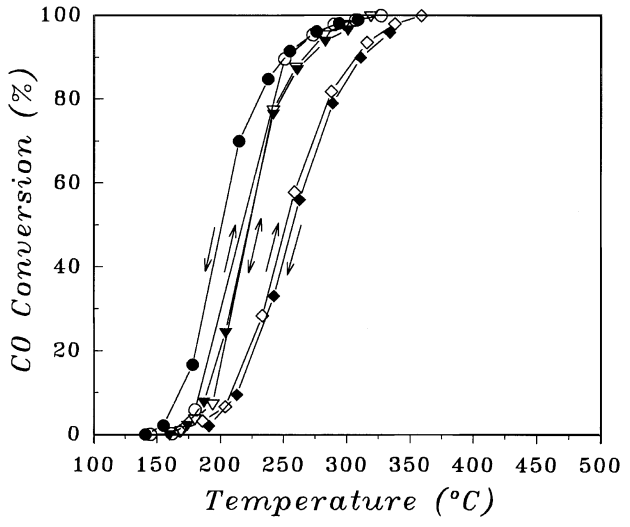

FIG. 6. Hysteresis phenomenon in the light-off test. Operation conditions are as in Fig. 5. Catalysts: (○, ●) chlorine-free 0.6 wt% Cu/YSZ; (▽, ▼) chlorine-containing 0.6 wt% Cu/YSZ; added amount of chlorine, 10 mol%; (◇, ◆) chlorine-containing 0.6 wt% Cu/YSZ; added amount of chlorine, 70 mol%. Open symbols, increasing temperature; filled symbols, decreasing temperature.

For the CuO/YSZ catalysts, the hysteresis loop can be observed in the light-off test as shown in Figs. 6 and 7. These results do not show behavior like the CuO/γ-alumina catalysts but rather like the PM catalysts as shown in Fig. 5. Hence, according to the hysteresis phenomena shown in Figs. 6 and 7, we conclude that the main mechanism for CO oxidation over the CuO/YSZ catalyst should not be the redox cycle one as mentioned above but a chemisorption-type one as proposed in this work (see Discussion) and in our previous study (12). This inference and anticipation will become more convincing by means of chlorine addition method in the next section.

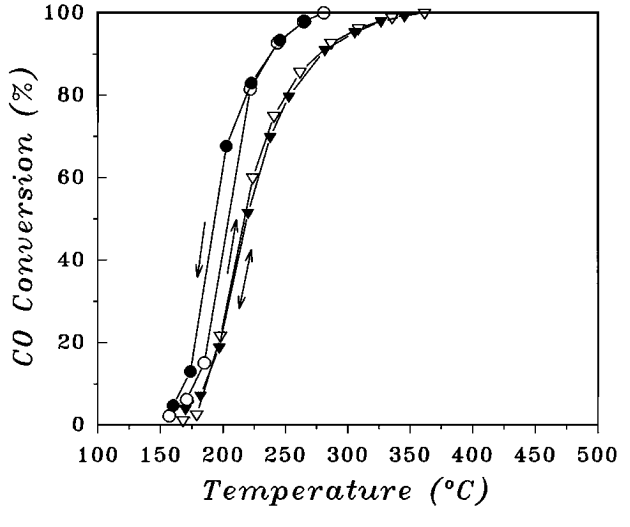

FIG. 7. Hysteresis phenomenon in the light-off test. Operation conditions: constant copper weight of 1.5 mg; the rest is the same as that of Fig. 5. Catalysts: (○, ●) chlorine-free 1.5 wt% Cu/YSZ; (▽, ▼) chlorine-containing 1.5 wt% Cu/YSZ; added amount of chlorine, 10 mol%. Open symbols, increasing temperature; filled symbols, decreasing temperature.

3.4 Chlorine Effect on CuO/YSZ Catalyst

It has been reported (44) that controlled addition of chlorine can lead to a two-step reduction of γ-alumina supported bulk-like CuO (i.e., $Cu^{2+} \rightarrow Cu^{+} \rightarrow Cu^{0}$). This should lead to two TPR peaks for bulky CuO reduction in CuO/γ-alumina. If the added amounts of chlorine were high enough, the two-step reduction would not take place any more but the reduction of the bulk-like CuO would occur at very high temperature (44). On the other hand, the highly dispersed copper oxide, especially isolated copper ions, are less affected by the added chlorine.

The TPR of chlorine-doped CuO/YSZ is similar to chlorine-doped CuO/γ-alumina. This result is shown in Fig. 8. It is seen that the γ-peak profiles of 0.6 and 1.5 wt% Cu/YSZ catalysts, of which the added amount of chlorine is 10 mol%, are similar to that of CuO/γ-alumina catalyst, of which the added amount of chlorine is 9.7 mol% (44), and also consist of γ_1 and γ_2 peaks. When the added amount of chlorine is increased to 70 mol%, there is only one TPR peak to be observed at very high temperature as shown in Fig. 8c. This reduction behavior of CuO/YSZ catalyst with

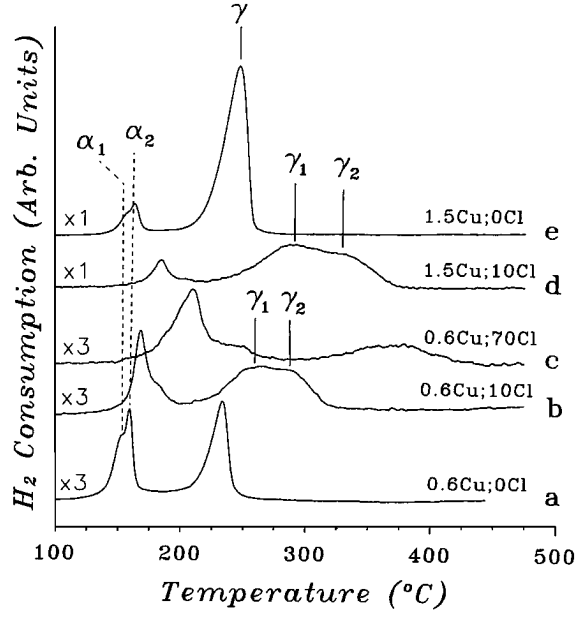

FIG. 8. TPR patterns of CuO/YSZ catalysts. Operating conditions: 10°C/min, 10% H_2 in N_2 with a total flow rate of 30 ml/min. Sample weight, 200 mg. Catalysts: (a) chlorine-free; copper loading, 0.6 wt%; (b) chlorine-containing; copper loading, 0.6 wt%; added amount of chlorine, 10 mol%; (c) chlorine-containing; copper loading, 0.6 wt%; added amount of chlorine, 70 mol%; (d) chlorine-containing; copper loading, 1.5 wt%; added amount of chlorine, 10 mol%; (e) chlorine-free; copper loading, 1.5 wt%; (γ) bulk-like CuO.

the high added amount of chlorine is also the same as that of the chlorine-added CuO/γ-alumina (44).

Figure 8 also shows that the α-peak temperature is shifted upward due to the addition of chlorine. It can be seen that the more chlorine added, the higher the α-peak temperature shift. Moreover, the α_1 and α_2 peaks have become indistinguishable owing to the chlorine addition. Obviously, the chlorine-added α-peak copper oxide species have a higher reduction temperature than the chlorine-free one; therefore, they should have different activities and catalytic behavior for CO oxidation.

Indeed, as shown in Figs. 6 and 7, the hysteresis loops disappear and the light-off characteristics also become increasingly degenerative and downfallen depending upon the shifted extent of α-peak temperature shown in Fig. 8. It is worth noting that as long as the shifted extent of α-peak temperature is not great, as in the case of Fig. 8b, the light-off behavior can still exist, although the profile of the γ peak has had an evident change. These suggest once again that the catalytic performance of CuO/YSZ catalyst is controlled by the α_1-peak copper oxide species instead of the $\beta + \gamma$-peak ones and the added chlorine can destroy the interfacial active centers composed of the α_1-peak copper oxide species and the surface oxygen vacancies of YSZ support. Consequently, the catalytic activity of chlorine-containing CuO/YSZ catalyst is lower than that of chlorine-free one, and the windows of the hysteresis loops are also closed due to the destruction of the interfacial active centers.

4. DISCUSSION

According to the early concept, the so-called "support" defined in catalysis such as SiO_2 is merely an inert substance which provides a means of spreading out an expensive catalyst ingredient such as platinum for its most effective use, or a means of improving the mechanical strength of catalyst. However, supports are not inert carriers any more in the phenomenon of SMSI. They cannot only modify the chemical properties of supported metals but also alter the mechanism and kinetics of reactions (1, 2, 15, 16). The enhancement of activity and selectivity due to the SMSI for CO hydrogenation can be regarded as the results of cooperation and synergy between metal and support. Similar cooperation or synergy between metal or metal oxide and support leading to the activity enhancement can also be found in other reactions such as CO oxidation (6, 7, 11, 14, 45, 46) and methanol oxidation (39). Their common feature is that the interfacial perimeter between the metal particle (or metal oxide particle) and support can provide new active centers, of which the TOF is very high.

The interfacial active centers which result from the cooperation and interaction between copper oxide and the YSZ support have also been proposed (12) and confirmed by TPR (40). Hence, in the following we intend to elucidate the importance of IMOSI in catalysis. The reasons for the remarkable activity enhancement of the YSZ supported copper oxide in contrast to the γ-alumina supported one and the probable mechanism for the genesis for the PM-like catalytic behavior will also be discussed according to the above results and the previous TPR and EPR results (40). In addition, a comparative discussion concerning the difference of reaction mechanism of CO oxidation over the PM, CuO/γ-alumina, and CuO/YSZ catalysts will also be given.

4.1 Active Site and Adsorption Behavior

It is well-known that if the reactants are very strongly adsorbed on the active sites, it will clearly be unreactive, as the chemisorption bond is too strong to be broken; on the other hand, if the molecules are so weakly adsorbed on the active sites that its coverage will be very low, then the catalytic rate will be at best minimal. This general principle is the so-called "Volcano Principle" (47).

When one comes to consider the more realistic case of two reactants, the situation will become somewhat complicated. In general, these will not be equally strongly chemisorbed, and one may assume that the rate will be proportional to the product of the fractional surface coverage of each (47). For instance, CO oxidation over PM catalyst is exactly the case. Its reaction rate can be expressed as (41, 43)

$$r = k\theta_{CO}\theta_O, \qquad [1]$$

where θ_{CO} is the coverage of CO and θ_O is the coverage of atomic oxygen. Thus when the two reactants fully cover the PM surface, the rate will be maximum when θ_{CO} equal θ_O (41, 43) and will depend critically on the variation of whichever is the smaller. At the moment, the active site will become a hot spot due to the exothermic reaction (48). Thus if the TOF of the active site is high enough, the catalytic reaction can be accelerated and subsist due to the heat generation from itself. Simultaneously, the reaction will become autocatalytic. Hence, a good active site should have a moderate strength of adsorption with respect to each of the reactants.

However, the adsorption strength of the active sites with respect to each reactant is always controlled and determined by the temperature. For the low temperature region first order with respect to oxygen and negative order with respect to CO were observed in CO oxidation over the PM catalysts (41, 49). On the other hand, when reaction ran into the high temperature region, the surface of PM catalyst was CO-free and was covered with adsorbed oxygen. Accordingly, kinetic orders of zeroth and first order with respect to oxygen and CO, respectively, were observed (41, 49). This explains why the maximum rate appears only at a certain temperature range (i.e., light-off temperature).

The adsorbed islands of oxygen are not synchronously desorbed from the PM catalyst surface during cooling until

the temperature is decreased to a certain one (43). A similar hysteresis behavior also occurs in the CO adsorption and desorption on the PM catalysts (50). These hysteresis phenomena are associated with the group-type adsorption and desorption behavior of CO and oxygen (41, 43, 50, 51). Therefore, when the reaction temperature is raised to a certain one, the adsorbed CO molecules which have formed islands will be desorbed in groups. Simultaneously, the gas phase oxygen has chance to be adsorbed in groups on the PM surface (41). Accordingly, the CO oxidation over the PM catalyst has the light-off behavior and hysteresis phenomenon as shown in Figs. 4 and 5.

For CO oxidation over the metal oxide catalyst, it was found that the reaction obeys mostly a redox cycle mechanism (49),

$$CO + O_{SL} \rightarrow CO_2 + \square_S \quad [2]$$

$$O_2 + 2\square_S \rightarrow 2O_{SL}, \quad [3]$$

where O_{SL} is a surface lattice oxygen and $\square_S$ is a surface oxygen vacancy on the oxide surface. Usually, reoxidation of the catalytic surface is rather fast and the first step of oxygen withdrawal from the metal oxide, i.e., reaction [2], appears to be the rate-determining step (18–20, 22, 28, 33–35, 49).

CO oxidation over CuO/γ-alumina catalyst is exactly the case as described by reactions [2] and [3]. Jernigan and Somorjai (34) pointed out that CO oxidation over CuO cata lyst belongs to a redox cycle mechanism between CuO and Cu_2O where the rate-limiting step is the reduction of copper (II) oxide by CO. Dekker and co-workers (37) also reported that CO oxidation over copper-based catalyst is considered to proceed according to an oxidation–reduction mechanism of the active phase. Possible redox couples under working conditions are Cu^+–Cu^{2+}, Cu^0–Cu^{2+} and Cu^0–Cu^+. After calcination in air copper is mainly present as Cu^{2+}. The oxidation state under oxygen-rich reaction condition is only slightly lower, which makes the redox couple Cu^+–Cu^{2+} the most probable for CO oxidation by oxygen (37).

From the viewpoint of chemisorption, chemisorbed oxygen is an electron acceptor, where electrons are donated from catalyst surface to the chemisorbed oxygen. Therefore, it is conceivable that oxygen will not dissociate on copper (II) oxide, because copper (II) oxide is an insulator and cannot donate electrons (34). This is to say that copper (II) oxide cannot provide an appropriate and good chemisorption site for oxygen adsorption. Hence, CO_2 production must result from the surface reduction of copper (II) oxide by CO (34).

Accordingly, the reaction kinetics of CO oxidation over copper oxide catalyst usually exhibit a positive-order dependence on CO and a zeroth-order dependence on oxygen (37, 52, 53), which is consistent with the rate expression of redox mechanism (54). Hence, increasing temperature does not significantly change the relative coverage of adsorbed species but mainly increases the reactivity and activity of the surface lattice oxygen of the γ-alumina supported copper oxide. These are the reasons why the CuO/γ-alumina catalyst does not have the light-off behavior in CO oxidation and hysteresis phenomenon in light-off test as shown in Figs. 4 and 5, respectively.

4.2 Interfacial Active Center and Oxygen Vacancy

In order to ameliorate the catalytic activity of PM catalyst which is inhibited by the strong adsorption of CO at low temperature, cerium oxide was used as support (6, 14) or additive (9, 11, 13, 46). The purpose of these catalyst designs was to provide a second pathway, which could supply oxygen to the reaction, after the PM surface had been fully covered with CO at low temperature. Consequently, the major reaction regime would be moved to the interfacial perimeter between metal particle and cerium oxide because CeO_2 could supply its interfacial lattice oxygen to take part in the reaction at very low temperature (6, 10, 14). An interfacial oxygen vacancy would thus be created after the interfacial lattice oxygen of cerium oxide had been removed by the interfacial metal-adsorbed CO (6, 10).

The interfacial oxygen vacancy would be a good site for oxygen adsorption even it could abstract the atomic oxygen of CO_2 and result in the reduction of CO_2 (6). More recently, Sale *et al.* (55) have given a theoretical discussion about the role of oxygen vacancies on ceria surfaces in the CO oxidation. They showed that the ready formation of oxygen vacancies on the (110) and (310) surfaces of CeO_2 significantly promotes the CO oxidation. The role of the interfacial active centers has been called the "metal–support interfacial reaction" (7, 12). The effect of the interfacial active centers, which are composed of the support interfacial oxygen vacancies and the active metal atoms, can be regarded as a sort of IMSI defined in literature (7, 15).

For CuO/YSZ catalyst, it has been confirmed that the NOI defined in our previous work (40) can be easily removed at ca. 150°C. Hence, a similar interfacial active center may be formed after the NOI reacts with CO to produce CO_2. Since our operation condition of activity test is oxygen-rich, Cu^+ instead of Cu^0 should be the stable species (34, 37, 56) after the NOI is removed by CO. This reaction step can be manifested by (illustrated in Fig. 9)

$$V_O^{\bullet\bullet}\cdots O^{2-}\cdots Cu^{2+}\text{–}O^{2-}\text{–}Cu^{2+} + CO \rightarrow V_O^{\bullet\bullet} + {}^{(V)}Cu^{+}\text{–}O^{2-}\text{–}Cu^{+} + CO_2, \quad [4]$$

where $V_O^{\bullet\bullet}$ is the oxygen vacancy of YSZ and $^{(V)}Cu^+$ is the reduced copper ion located beside the oxygen vacancy of YSZ. Hence, the interfacial active center on CuO/YSZ catalyst is composed of the $V_O^{\bullet\bullet}$ and the $^{(V)}Cu^+$.

Many studies have reported that CO prefers to adsorb on Cu^+ (56–59), especially on Cu^+ in a Cu^{2+} matrix (60, 61), rather than Cu^0 (57, 61, 62). This chemisorption character of CO, which prefers to adsorb on *p*-type semiconducting

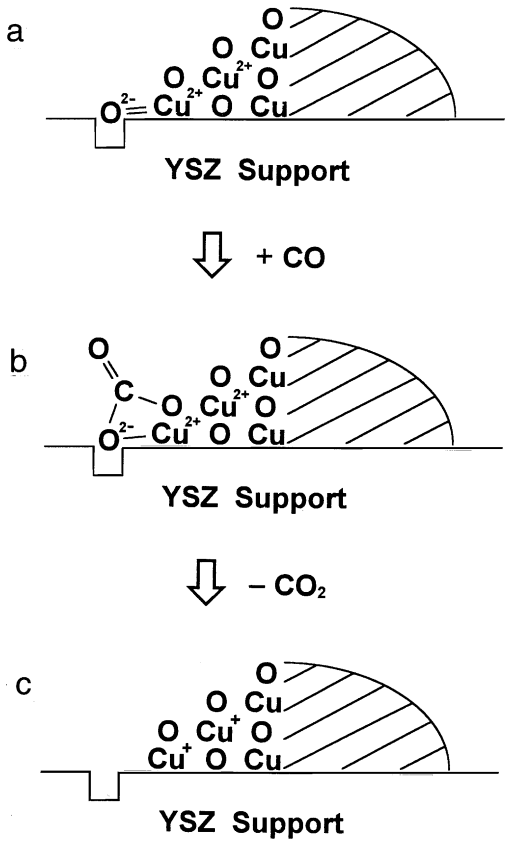

FIG. 9. Scheme of interfacial active center formation. (⌐¬) Surface oxygen vacancy of YSZ support, (▨) Copper oxide particle.

oxide (33, 63) such as Cu_2O (64), is due to the lone pair of electrons on carbon, which has a high degree of *p* character and results in a donor-type chemisorption behavior (65). Accordingly, the *p*-type semiconducting oxide, e.g., Cu_2O, which can supply the electron holes, will give a higher activity for the donor-type reaction of CO (63).

In our previous work (12), we have proposed that once the $^{(V)}Cu^{+}$ is formed, it can no longer be easily reduced or oxidized because there is an oxygen vacancy of YSZ existing beside it. In other words, the oxygen vacancy can "protect" the interfacial $^{(V)}Cu^{+}$ from further reduction or oxidation. Therefore, the interfacial active center of CuO/YSZ catalyst can be stabilized during reaction.

On the other hand, Zhang *et al.* (66) pointed out that these oxygen vacancies of oxygen-ion conducting solids (e.g., YSZ) may make suitable sites available for oxygen adsorption. The chemisorption of oxygen on oxygen-ion conducting solids may result in a mixture of various oxygen species (e.g., O_2^-, O_2^{2-}, O^-) on the surface. The chemisorption of oxygen on oxygen-ion conducting oxides can be expressed as (66)

$$O_{2(g)} + V_O^{\cdot\cdot} + e^- \rightleftharpoons \text{adsorbed oxygen } \left(O_2^-, O_2^{2-}, O^-\right), \quad [5]$$

where e^- is the quasi-free electron. It may also be available via the reduction of surface lattice oxygen O^{2-}, i.e., $O^{2-} \rightarrow O^- + e^-$ (66). Zhang *et al.* (66) further reported that as the concentration of oxygen defects increases, the surface ions may donate their electrons to neighboring surface anionic vacancies, which then react with the gaseous oxygen,

$$1/2O_{2(g)} + O^{2-} + V_O^{\cdot\cdot} \rightarrow 2O_O^x, \quad [6]$$

where O_O^x is the atomic oxygen. More recently, a similar adsorption mechanism as described by Eq. [6] is also proposed by Lacombe and co-workers (67). The common features of oxygen chemisorption on the oxygen-ion conducting materials may be (i) the high capacity for oxygen adsorption; and (ii) the tendency to form atomic-type oxygen species on the surface (66).

In fact, the oxygen vacancies of YSZ have been verified to be good adsorbing sites for the adsorption of SO_3 and CO (24) and to be active sites for CO hydrogenation (25) and C_4 synthesis (26) as well as acting as defect sites for oxygen adsorption. As to the oxygen species adsorbed on the oxygen vacancy of YSZ, we cannot give an unambiguous determination only in the light of our current data. Nevertheless, based on the conclusion as mentioned above, the atomic-type oxygen species is preferable and will be designated as $^{(V)}O_{(ad)}$ in subsequent discussion.

Based on the above discussion, the interfacial active center composed of $V_O^{\cdot\cdot}$ and $^{(V)}Cu^{+}$ caused by the IMOSI is a good and proper site for CO oxidation according to the Volcano Principle. As the similar effect of cerium oxide on the PM catalyst as mentioned above, it also provides a second pathway which supplies a chemisorbed oxygen instead of a lattice oxygen to take part in the reaction, and thus results in the activity enhancement of copper oxide. This rate-determining step can be expressed as Eq. [8] in

$$CO_{(g)} + {}^{(V)}Cu^{+} \rightleftharpoons {}^{(V)}Cu^{+}\cdots CO_{(ad)} \quad [7]$$

$$^{(V)}O_{(ad)} + {}^{(V)}Cu^{+}\cdots CO_{(ad)} \rightarrow V_O^{\cdot\cdot} + {}^{(V)}Cu^{+} + CO_2, \quad [8]$$

where $CO_{(ad)}$ denotes the adsorbed CO. According to the activity test results shown in Fig. 4, one may imagine that the TOF of reaction [8] is much higher than that of reaction [2]. Hence, as shown in Fig. 3, the catalytic performance of CuO/YSZ catalyst is not only dependent on but also controlled by the amounts of α_1-peak copper oxide species, i.e., the numbers of the interfacial active center. However, the contribution of reaction [2] in CO oxidation cannot be completely neglected, especially for a high copper loading one, according to the results shown in Fig. 2.

Obviously, the key points for occasion of the light-off behavior in the CO oxidation over the CuO/YSZ catalyst are reactions [4] and [8]. That is, first, the formation of the interfacial active center and, then, fast turnover of the adsorbed reactants by the interfacial active center. As a result, the

interfacial active center can become a hot spot due to the high TOF of reaction [8]. Thus, this will cause the reaction [8] to proceed increasingly faster and become autocatalytic and finally to show the light-off behavior during heating. Therefore, the formation of hysteresis loop can be reasonably attributed to that the $^{(V)}Cu^{+}$ can be stabilized by the $V_O^{\cdot\cdot}$ as mentioned above. Hence, the interfacial active center will not disappear at once during cooling until $^{(V)}Cu^{+}$ returns to its original state, i.e., Cu^{2+}, owing to the temperature being decreased enough. This argument will become more convincing by means of chlorine addition on the CuO/YSZ catalyst and is further discussed in the next section.

4.3. Effect of Chlorine Addition

In our previous study (40), we have provided evidence that the α peak formation in the TPR patterns of CuO/YSZ catalyst is associated with the surface oxygen vacancies of YSZ support. All the interpretations presented in previous work (40) are based on a major premise that the oxygen vacancies exist at the surface of YSZ support and enhance the reducibility of CuO. Hence, one can imagine that if the surface oxygen vacancies of YSZ support can be blocked from inducing the removal of NOI via reduction mechanism I proposed in Part I of this work (40), then the α_1 peak should disappear in the TPR pattern.

It has been mentioned that the surface oxygen vacancies of YSZ are good adsorbing sites, hence one of the methods that can block the oxygen vacancies or may invalidate their induction function is poisoning them. Essentially, the principle of poisoning mechanism of the oxygen vacancy is similar to that of metal atoms. For metal atoms, especially transition metals, they have unoccupied orbitals, which can accept electrons from chemisorbing species, hence the compounds of sulfur and chlorine that have lone pairs of electrons may be strongly adsorbed. For oxygen vacancies of YSZ, they possess positive charge (68, 69), which can act as Lewis acid site (25, 70), thus the compounds of sulfur and chlorine may also be adsorbed strongly on the oxygen vacancies.

If fact, Munuera and co-workers (71) have confirmed that chlorine atoms generated during decomposition of the precursor ($RhCl_3$) may be trapped by the oxygen vacancies of TiO_2 support. They also concluded that once the chlorine atoms are incorporated into the oxygen vacancies, an extensive reduction of TiO_2 support is difficult. This may justify the observation by Bond *et al.* (72) and Guenin *et al.* (73) that chlorine inhibits or retards the SMSI state. This effect can be related to the filling of surface oxygen vacancies by the chlorine, thus retarding the reduction of the TiO_2, CeO_2 and Nb_2O_5 supports.

Indeed, as shown in Figs. 8b and 8d, it is obvious that after chlorine was added on the CuO/YSZ catalysts, the α_1 peak had disappeared and the so-called α peak had become a high temperature one as compared with the original α peak appearing in Figs. 8a and 8e. As a result, both the light-off behavior and the hysteresis loop in activity test also disappear as shown in Figs. 6 and 7. Recalling the two key points, the interfacial $^{(V)}Cu^{+}$ and $V_O^{\cdot\cdot}$, which result in the light-off behavior and the hysteresis phenomenon, all the effects of the chlorine addition on the TPR behaviors and the catalytic activities can be rationally explained as follows.

When the chlorine is added on the CuO/YSZ catalyst, the surface oxygen vacancies of YSZ support will be blocked by the adsorbed chlorine at low temperature. As a result, the NOIs may thus become nested chlorines at low reduction temperature. In addition, it should be emphasized that the added chlorine may also exist in the supported crystallite behaving as dopant (44, 74). These chlorine dopants can cause the reduction of crystalline copper oxide to be difficult due to a "long-range" electronic effect (44). Since the removal of the chlorines that are adsorbed on the $V_O^{\cdot\cdot}$ and that exist in the copper oxide particles are difficult, the interfacial copper oxides can be reduced only at higher temperature after the $V_O^{\cdot\cdot}$-adsorbed chlorines are removed by hydrogen.

According to the TPR patterns of Figs. 8b and 8d, it can be inferred that the $V_O^{\cdot\cdot}$-adsorbed chlorines should be removed more easily at higher reduction temperatures than exist in the supported copper oxide particles. This is to say that the $V_O^{\cdot\cdot}$-adsorbed chlorines are prior removed during reduction; subsequently, the NOI and TOI reduction mechanism proposed in our previous work (40) may thus proceed owing to the restoration of the surface oxygen vacancies of YSZ support. Nevertheless, at the moment, these chlorines doped in the copper oxide particles are not yet removed by hydrogen. Consequently, the $V_O^{\cdot\cdot}$ effect on the interfacial copper oxide reduction results in the shifted α-peak formation as shown in Figs. 8b, 8c, and 8d.

On the other hand, using the temperature-programmed oxidation (TPO), it has been demonstrated (44) that the reduced metal copper can be easily reoxidized due to the presence of chlorine. The higher the amount of residual chlorine, the lower the TPO peak temperature of the reduced metal copper obtained (44). Accordingly, the window of the hysteresis loop is closed by the $^{(V)}Cu^{+}$ being easily reoxidized to Cu^{2+} during cooling due to the chlorine effect. In other words, the disappearance of the hysteresis phenomenon caused by the chlorine addition can be attributed to the interfacial active center proposed in Section 4.2 not being able to be held during cooling.

It has been reported (44) that the reduction of the isolated Cu^{2+} ions is less affected by the chlorine addition. Hence, the shift of α-peak temperature caused by the chlorine addition may exactly show that the α-peak copper oxide species are not the isolated copper ions but the weak magnetic associates of copper ions or the small two- and three-dimensional clusters, of which the reduction behavior

can be altered by the doped chlorine. This result is coincident with the EPR spectra (40).

As to the adsorbed type of chlorine, we cannot depend merely upon current data to give a determination. However, Munuera *et al*. (71) and Bond *et al*. (72, 75) have reported that chlorine ions and chlorine atoms both are the usual types adsorbed on the support.

4.4 Characterization of Active Species

So far, we have pointed out and proposed where the active center is and what reaction mechanism is operative for the CuO/γ-alumina catalyst and the CuO/YSZ catalyst, respectively. Subsequently, we will discuss what kind of structure and environment of the active species of interest is dominant.

In fact, the structure and coordination environment of the γ-alumina supported copper oxide have been thoroughly studied by many authors using many physical methods (76–81). According to the literature (76–81), the copper–oxygen entities supported on the γ-alumina can be classified into several types: *(a) isolated Cu^{2+} ions; (b) weak magnetic associates; (c) small two-and three-dimensional clusters; (d) large three-dimensional clusters and bulk CuO phase.* Their characters and chemical and physical properties have been detailedly described in the Part I (40) of this work.

In our previous study (40), the TPR and EPR results have confirmed that the γ-peak copper oxide species belong to type *(d)* and the β-peak copper oxide species are composed of types *(a), (b),* and *(c)*. Comparing the intensities of EPR signals and considering their hyperfine structure shown in our previous work (40), it can be safely concluded that the most active species in the β-peak copper oxide species are type *(c)* as described above. This also coincides with the results reported by Davydova *et al*. (60) and Tikhov and co-workers (77), in which small two- and three-dimensional clusters are the most reactive species.

On the other hand, for the CuO/YSZ catalysts, it has also been verified (40) that the α_1-peak generation is not due to the reduction of the isolated Cu^{2+} ions but the hydrogen uptake of NOIs, which are the interface-boundary terminal oxygen ions of which the coordination environment belongs to types *(b), (c)*, or *(d)* as illustrated in Fig. 9a. Hence, both the NOIs and the TOIs defined in our previous work (40) are the oxygen ions of types *(b), (c)*, or *(d)* copper oxide species. This also agrees with the results of chlorine addition that the α-peak temperature can be markedly shifted by the added chlorine, which indicates that the α-peak copper oxide species are not isolated copper ions.

Consequently, comparing Figs. 8b and 8d, the shifted extent of the α-peak temperature of the 1.5 wt% Cu/YSZ catalyst being greater than that of 0.6 wt% one can be rationally attributed to the different particle size of the supported copper oxide. The higher the copper loading is, the larger the particle size will be and the more residual chlorine that can exist in the copper oxide microcrystallites, which leads to a stronger electronic effect on reduction. Hence, when the added amount of chlorine is increased to 70 mol% on the 0.6 wt% Cu/YSZ catalyst, there is a much more serious temperature shift as shown in Fig. 8c.

5. CONCLUSIONS

1. Catalytic activity of copper oxide catalyst for CO oxidation can be significantly enhanced by the oxygen-ion conducting support, YSZ, which leads to the supported copper oxide exhibiting a PM-like catalytic behavior.

2. The activity enhancement of the YSZ supported copper oxide is attributed to the surface oxygen vacancy of YSZ support providing a second reaction pathway by means of the formation of interfacial active center, although the redox cycle mechanism is still operative on the CuO/YSZ catalyst.

3. The interfacial active center of the CuO/YSZ catalyst is formed by the IMOSI and composed of the interfacial Cu^+ ion and the surface oxygen vacancy of YSZ support. These interfacial active centers exhibit the chemisorption-type reaction mechanism instead of the redox cycle one.

4. The interfacial active center of CuO/YSZ catalyst can be destroyed by the chlorine addition, which leads to the disappearance of light-off behavior and the close of hysteresis loop in the activity test and to the temperature shift of the α peak in the TPR patterns of CuO/YSZ toward higher one. These are ascribed to the occupancy of the surface oxygen vacancy of YSZ by the strongly adsorbed chlorine and the easy reoxidization of the interfacial Cu^+ ion due to the electronic effect of the added chlorine.

ACKNOWLEDGMENTS

This work was supported by the National Science Council of Republic of China under Contract NSC 83-0402-E-007-006. We are thankful to Mr. Yu-Piao Wang for the catalyst preparation. We thank the reviewers of this paper for giving many valuable and helpful comments and modifications.

REFERENCES

1. Stevenson, S. A., Dumesic, J. A., Baker, R. T. K., and Ruckenstein, E. (Eds.), "Metal-Support Interaction in Catalysis, Sintering, and Redispersion." Van Nostrand–Reinhold, New York, 1987.
2. Haller, G. L., and Resasco, D. E., *Adv. Catal.* **36**, 173 (1989).
3. Summers, J. C., and Ausen, S. A., *J. Catal.* **58**, 131 (1979).
4. Yao, H. C., and Yu Yao, Y. F., *J. Catal.* **86**, 254 (1984).
5. Diwell, A. F., Rajaram, R. R., Shaw, H. A., and Truex, T. J., *in* "Catalysis and Automotive Pollution Control II" (A. Crucq, Ed.), p. 139. Elsevier, Amsterdam, 1991.
6. Jin, T., Okuhara, T., Mains, G. J., and White, J. M., *J. Phys. Chem.* **91**, 3310 (1987).
7. Metcalfe, I. S., and Sundaresan, S., *AIChE J.* **34**, 195 (1988).
8. Munuera, G., Fernandez, A., and Gonzalez-Elipe, A. R., *in* "Catalysis and Automotive Pollution Control II" (A. Crucq, Ed.), p. 207. Elsevier, Amsterdam, 1991.

9. Lööf, P., Kasemo, B., Andersson, S., and Frested, A., *J. Catal.* **130**, 181 (1991).
10. Serre, C., Garin, F., Belot, G., and Maire, G., *J. Catal.* **141**, 1 (1993).
11. Serre, C., Garin, F., Belot, G., and Maire, G., *J. Catal.* **141**, 9 (1993).
12. Dow, W.-P., and Huang, T.-J., *J. Catal.* **147**, 322 (1994).
13. Yu Yao, Y. F., *J. Catal.* **87**, 152 (1984).
14. Zafiris, G, S., and Gorte, R. J., *J. Catal.* **143**, 86 (1993).
15. Burch, R., and Flambard, A. R., *J. Catal.* **78**, 389 (1982).
16. Vannice, M. A., and Sudhakar, C., *J. Phys. Chem.* **88**, 2429 (1984).
17. Sanchez, M. G., and Gazquez, J. L., *J. Catal.* **104**, 120 (1987).
18. Roozeboom, F., Jos van Dillen, A., Geus, J. W., and Gellings, P. J., *Ind. Eng. Chem. Prod. Res. Dev.* **20**, 304 (1981).
19. van den Berg, J., Brans-Brabant, J. H. L. M., van Dillen, A. J., Geus, J. W., and Lammers, M. J. J., *Ber. Bunsenges. Phys. Chem.* **87**, 1204 (1983).
20. Severino, F., and Laine, J., *Ind. Eng. Chem. Prod. Res. Dev.* **22**, 396 (1993).
21. Boon, A. Q. M., van Looij, F., and Geus, J. W., *J. Mol. Catal.* **75**, 277 (1992).
22. Klissurski, D., and Rives, V., *Appl. Catal. A* **109**, 1 (1994).
23. Belapurkar, A. D., Gupta, N. M., Phatak, G. M., and Iyer, R. M., *J. Mol. Catal.* **87**, 287 (1994).
24. Silver, R. G., Hou, C. J., and Ekerdt, J. G., *J. Catal.* **118**, 400 (1989).
25. Jackson, N. B., and Ekerdt, J. G., *J. Catal.* **126**, 31 (1990).
26. Jackson, N. B., and Ekerdt, J. G., *J. Catal.* **126**, 46 (1990).
27. Hightower, J. W., *in* "Preparation of Catalysts I" (B. Delmon, P. A. Jacobs, and G. Poncelet, Eds.), p. 615. Elsevier, Amsterdam, 1976.
28. Kummer, J. T., *Prog. Energy Combust. Sci.* **6**, 177 (1980).
29. Huang, T.-J., Yu, T.-C., and Chang, S.-H., *Appl. Catal.* **52**, 157 (1989).
30. Huang, T.-J., and Yu, T.-C., *Appl. Catal.* **71**, 275 (1991).
31. Stegenga, S., van Soest, R., Kapteijn, F., and Moulijn, J. A., *Appl. Catal. B* **2**, 257 (1993).
32. Boccuzzi, F., Guglielminotti, E., Martra, G., and Cerrato, G., *J. Catal.* **146**, 449 (1994).
33. Bielañski, A., and Haber, J., "Oxygen in Catalysis," p. 244. Dekker, New York, 1991.
34. Jernigan, G. G., and Somorjai, G. A., *J. Catal.* **147**, 567 (1994).
35. Golodets, G. I., "Heterogeneous Catalytic Reactions Involving Molecular Oxygen," p. 280. Elsevier, Amsterdam, 1983.
36. Severino, F., Brito, J., Carias, O., and Laine, J., *J. Catal.* **102**, 172 (1986).
37. Dekker, N. J. J., Hoorn, A. J. J., Stegenga, S., Kapteijn, F., and Moulijn, J. A., *AIChE J.* **38**, 385 (1992).
38. Praserthdam, P., and Majitnapakul, T., *Appl. Catal. A* **108**, 21 (1994).
39. Deo, G., and Wachs, I. E., *J. Catal.* **146**, 323 (1994).
40. Dow, W.-P., Wang, Y.-P., and Huang, T.-J., *J. Catal.*, **160**, 155 (1996).
41. Engel, T., and Ertl, G., *Adv. Catal.* **28**, 1 (1979).
42. Berlowitz, P. J., Peden, C. H. F., and Goodman, D. W., *J. Phys. Chem.* **92**, 5213 (1988).
43. Boudeville, Y., and Wolf, E. E., *Surf. Sci.* **297**, L 127 (1993).
44. Dow, W.-P., and Huang, T.-J., *Appl. Catal.*, in press.
45. Haruta, M., Tsubota, S., Kobayashi, T., Kageyama, H., Genet, M. J., and Delmon, B., *J. Catal.* **144**, 175 (1993).
46. Oh, S. H., and Eickel, C. C., *J. Catal.* **112**, 543 (1988).
47. Bond, G. C., "Heterogeneous Catalysis: Principle and Applications," 2nd ed., p. 62. Oxford Univ. Press, New York, 1987.
48. Schweich, D., and Leclerc, J. P., *in* "Catalysis and Automotive Pollution Control II" (A. Crucq, Ed.), p. 437. Elsevier, Amsterdam, 1991.
49. Boreskov, G. K., *in* "Catalysis: Science and Technology" (J. R. Anderson and M. Boudart, Eds.), Vol. 3, p. 40. Springer-Verlag, Berlin, Heidelberg, 1982.
50. Jackman, T. E., Griffiths, K., Davies, J. A., and Norton, P. R., *J. Chem. Phys.* **79**, 3529 (1983).
51. Jorgensen, S. W., and Madix, R. J., *Surf. Sci.* **163**, 19 (1985).
52. Blumenthal, J. L., and Nobe, K., *Ind. Eng. Chem. Proc. Des. Dev.* **5**, 177 (1966).
53. Yu Yao, Y. F., *J. Catal.* **39**, 104 (1975).
54. Satterfield, C. N., "Heterogeneous Catalysis in Industrial Practice," 2nd ed., p. 269. McGraw–Hill, New York, 1991.
55. Sayle, T. X. T., Parker, S. C., and Catlow, C. R. A., *Surf. Sci.* **316**, 329 (1994).
56. Choi, K. I., and Vannice, M. A., *J. Catal.* **131**, 22 (1991).
57. Miró, E. E., Lombardo, E. A., and Petunchi, J. O., *J. Catal.* **104**, 176 (1987).
58. Bijsterbosch, J. W., Muijsers, J. C., van Langeveld, A. D., Kapteijn, F., and Moulijn, J. A., *in* "Fundamental Aspects of Heterogeneous Catalysis Studied by Particle Beams" (H. H. Brongersma and R. A. van Santen, Eds.), p. 221. Plenum, New York, 1991.
59. Bijsterbosch, J. W., Kapteijn, F., and Moulijn, J. A., *J. Mol. Catal.* **74**, 193 (1992).
60. Davydova, L. P., Fenelonov, V. B., Sadykov, V. A., Plyasova, L. M., and Anufrienko, V. F., *Kinet. Catal.* **34**, 85 (1993).
61. Padley, M. B., Rochester, C. H., Hutchings, G. J., King, F., *J. Catal.* **148**, 438 (1994).
62. London, J. W., and Bell, A. T., *J. Catal.* **31**, 32 (1973).
63. Doshi, R., Alcock, C. B., Gunasekaran, N., and Carberry, J. J., *J. Catal.* **140**, 557 (1993).
64. Rakhshani, A. E., *Solid-State Electron.* **29**, 7 (1986).
65. Orrchin, M., and Jaffé, H. H., "The Importance of Antibonding Orbitals," p. 32. Houghton Mifflin, Boston, (1967).
66. Zhang, Z., Verykios, X. E., and Baerns, M., *Catal. Rev. Sci. Eng.* **36**, 507 (1994).
67. Lacombe, S., Geantet, C., and Mirodatos, C., *J. Catal.* **151**, 439 (1994).
68. Subbarao, E. C., Ed., "Solid Electrolytes and Their Applications." Plenum, New York, 1980.
69. Subbarao, E. C., and Maiti, H. S., *Solid State Ionics* **11**, 317 (1984).
70. Méthivier, A., and Pijolat, M., *J. Catal.* **139**, 329 (1993).
71. Munuera, G., Gonzalez-Elipe, A. R., Espinos, J. P., Muñoz, A., Conesa, J. C., Soria, J., and Sanz, J., *Catal. Today* **2**, 663 (1988).
72. Bond, G. C., Rajaram, R. R., and Burch, R., *J. Phys. Chem.* **90**, 4877 (1986).
73. Guenin, M., Da Silva, P. N., and Frety, R., *Appl. Catal.* **27**, 313 (1986).
74. Lieske, H., Lietz, G., Spindler, H., and Völter, J., *J. Catal.* **81**, 8 (1983).
75. Bond, G. C., Namijo, S. N., and Wakeman, J. S., *J. Mol. Catal.* **64**, 305 (1991).
76. Berger, P. A., and Roth, J. F., *J. Phys. Chem.* **71**, 4307 (1967).
77. Tikhov, S. F., Sadykov, V. A., Kryukova, G. N., Paukshtis, E. A., Popovskii, V. V., Starostina, T. G., Kharlamov, G. V., Anufrienko, V. F., Poluboyarov, V. F., Razdobarov, V. A., Bulgakov, N. N., and Kalinkin, A. V., *J. Catal.* **134**, 506 (1992).
78. Lumbeck, H., and Voitländer, J., *J. Catal.* **13**, 117 (1969).
79. Deen, R., Scheltus, P. I. T., and de Vries, G., *J. Catal.* **41**, 218 (1976).
80. Friedman, R. M., Freeman, J. J., and Lytle, F. W., *J. Catal.* **55**, 10 (1978).
81. Strohmeier, B. R., Leyden, D. E., Scott Field, R., and Hercules, D. M., *J. Catal.* **94**, 514 (1985).